Measurement of Charge Distribution around a Rising Bubble in a 2-D Fluidized Bed

Aihua Chen, Hsiaotao T. Bi, and John R. Grace
Dept. of Chemical and Biological Engineering, University of British Columbia, Vancouver V6T 1Z4, Canada

Flip Kleijn van Willigen and J. Ruud van Ommen
DelftChemTech, Delft University of Technology, Julianalaan 136, 2628 BL Delft, The Netherlands

DOI 10.1002/aic.10609
Published online September 7, 2005 in Wiley InterScience (www.interscience.wiley.com).

A technique has been developed to determine the charge distribution around single rising bubbles in a two-dimensional fluidized bed. Four induction probes positioned flush with the outside wall of the column and connected to charge amplifiers record induced charge signals as bubbles pass. The charge distribution surrounding a single bubble is then reconstructed with the assumption that the bubble is symmetrical and that the charge around the bubble remains constant as it rises. The emulsion phase far from the bubble in a two-dimensional fluidized bed of glass beads was found to be charged negatively and, contrary to our previous assumptions, the charge density decreased gradually toward the bubble-dense phase interface, with a nearly zero charge density inside the bubble. The wake of the bubble is more negatively charged than the emulsion phase, supporting our previous speculations. © 2005 American Institute of Chemical Engineers *AIChE J,* 52: 174–184, 2006

Keywords: triboelectric charging, particles, electrostatics, gas–solid fluidized beds, bubbles, induction probes

Introduction

Electrostatic charging in gas–solid fluidized beds is unavoidable. When the discharging rate of the particles is low compared to the charging rate, the negative effects on fluidization can induce problems such as particle agglomeration, changes in the hydrodynamic behavior of the bed, adhesion of particles to the walls, interference with instruments, nuisance discharges or explosions, and undesirable by-products.

The source of charge generation in fluidized beds is the contact and separation between particles, the fluidizing gas, and the reactor wall in which they are contained. This process is known as *triboelectrification*.[1] When the particles are insulators (such as sand, glass, FCC catalyst, polymers, many pharmaceutical materials) and the fluidizing gas has low conductivity (that is, low relative humidity in the case of air) the discharge rate is typically much lower than the charging rate, leading to a buildup of electrostatic charges in the system. In fluidization, we can differentiate between particle–particle and particle–wall contacts. Because particle–particle collisions result only in a separation of charge, the net charge over the two particles is conserved. Which particle gains or loses charge is difficult to predict when they are similar in size and material. This is different when fluidizing dissimilar materials (that is, blends of particles of binary particle sizes); there will usually be a clear preference for one group to be charged differently than the other group in a process known as bipolar charging.[2]

The collision of particles with the reactor wall, on the other hand, always occurs between dissimilar materials. When this is the case, there is typically a net flow of charge to or from the walls. Thus, whereas particle–particle interaction does not lead to an overall charge buildup in a fluidized bed, particle–wall collisions will. Charging by the fluidizing gas is generally considered to be low[3] unless ionized gas is used. Despite the

Correspondence concerning this article should be addressed to H. T. Bi at xbi@chml.ubc.ca.

negative effects of charge buildup, the mechanisms of charge generation and dissipation remain poorly understood.

The buildup of net charges in the bed has been studied using Faraday pails (see Chen et al.[4] for an overview) or induction systems.[5] However, a bubbling fluidized bed consists of two distinct phases: a dense phase (also known as emulsion phase) and a dispersed bubble phase. The reactant concentration is usually higher in bubbles and the region surrounding bubbles, leading to faster reaction near the bubbles than elsewhere in the dense phase. Particles in the region surrounding a rising bubble tend to move more quickly than particles elsewhere in the dense-phase region of the bed. Particle–particle and particle–wall collisions are more vigorous among particles surrounding bubbles, potentially leading to higher rates of charge generation arising from particle–particle contact charging. It is therefore expected that particles around bubbles may carry higher charges than those further away.

Until recently, there have only been two studies in the open literature on electrostatic charges around bubbles in fluidized beds. Based on the signals from an induction probe, Boland and Geldart[6] speculated that the front and wake of bubbles carry charges of opposite signs. A collision probe inside a two-dimensional column was used by Park et al.[7] to explore charge induction and transfer when a single bubble passed. Park et al.[8] and Chen et al.[9] developed a theoretical model to explain the electrical current signals generated by the passing of single gas bubbles. The model, which assumes that there is a charge distribution in the region adjacent to the bubble and much higher charge density in the wake region of the same sign as the front region of the bubble, correctly predicted the trend of charge signals registered by a sensitive collision probe when bubbles passed. Testing of the quantitative predictions from this model requires information on the distribution of specific charge density surrounding rising gas bubbles in gas–solids fluidized beds. Examining the distribution of charges in the vicinity of rising bubbles can assist in understanding electrostatic charge generation, charge separation, dissipation, and accumulation in fluidized bed reactors.

The purpose of this study was to develop a technique to measure the charge distribution surrounding a single rising bubble in two-dimensional gas–solids fluidized beds. The new technique is independent of net charge buildup in the bed, not influenced by charge transfer such as with collision probes, and allows the reconstruction of the complete charge distribution around bubbles, unlike the line traces or averages available from other techniques. Induction probes, which have been widely used for the measurement of surface charge distribution with high spatial resolution,[10] were selected to measure the charge distribution around rising bubbles in two-dimensional columns made of transparent materials. A number of induction probes were placed flush with the outer surface of the column to eliminate probe interference with the motion in the bed and charge transfer arising from collisions between particles and the probe. These induction probes are sensitive to *changes* in electric field as a bubble passes, and as such are not influenced by residual charge on the column wall. Signals from the probes are analyzed using an image-reconstruction technique to map the charge distribution around the bubble, which is independent of a priori knowledge of the bubble size or location. The resolution of the reconstruction is affected by the size and number of probes. In this investigation, four probes were used.

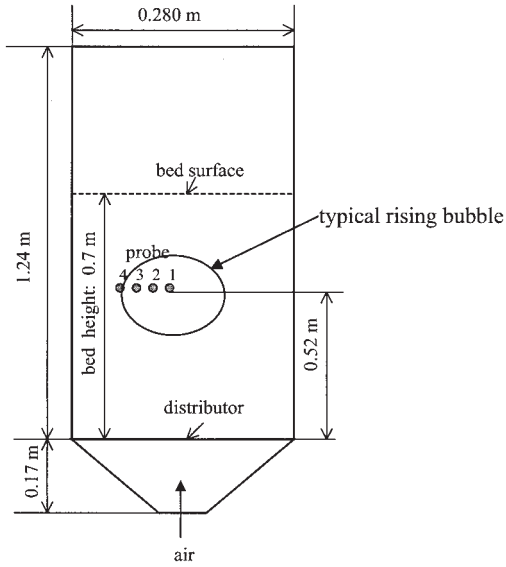

Figure 1. Front view of the two-dimensional fluidization column, showing the optimal location and size of a bubble rising by the induction probes.

Measurement Technique

Tests on the static charge around bubbles were conducted with induction probes in a two-dimensional fluidized bed. The column, made of Plexiglas®, has an inner thickness of 14 mm, a width of 280 mm, and a height of 1.24 m. The windbox volume is 800 cm^3. Glass beads of diameter 0.560 mm and density 2500 kg/m^3 were used as the bed material. The settled bed height was approximately 700 mm. The bed was fluidized at an air flow rate of $Q_{air} = 1.78 m^3/s$, leading to a regular pattern of independent bubbles with few particles raining through them. Bubbles were approximately 80 mm in diameter and had rise velocities of about 0.26 m/s. Figure 1 shows a schematic of the column and probes. Copper tape on both the front and rear walls was connected to ground to maintain a zero potential on the column wall. The resistivity between the left and right sides of the column was measured to be $3.8 \times 10^7\ \Omega\ m^{-1}$. Four induction probes were placed 520 mm above the perforated plate distributor. The distance between adjacent probes was 13 mm. A Canon digital video camera, operating at 30 frames/s, was used to record the rise of bubbles through the column and to ensure that measurements were performed on single bubbles not directly influenced by others. Bubbles whose center passed probe 1 and whose edge passed probe 4 were selected for further analysis. The video was thus always synchronized to the charge measurements.

Induction probes (see Figure 2) constitute the simplest type of field meters. Each induction probe consists of an insulated, circular copper disc (10 mm diameter), connected to the core of a coaxial cable, embedded in a Teflon® cylinder, and wrapped with a single strip of conducting copper tape. The shielding of the coaxial cable is connected to the shielding around the probe and to the common ground that, together with the coated and grounded walls of the column, minimizes distortion of the signal from charges above, below, or to the side of the probe. The metal sensor is charged by induction attributed to the electric field generated by the charged particles.

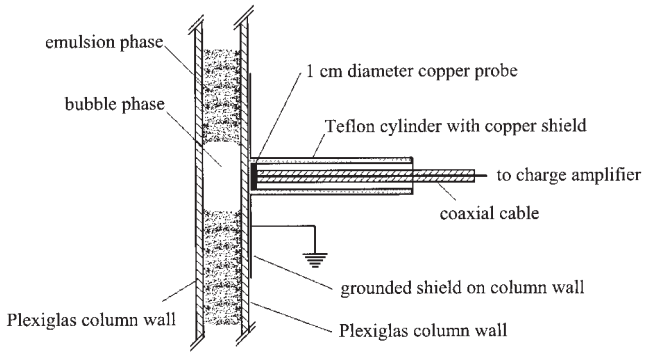

Figure 2. Induction probe.

The probe is placed flush with the outside wall of the column (as shown). Around the probe and on the column wall is the grounded shielding. When a bubble is in front of the probe, little or no charge is induced on it. When the bubble passes past the probe, the charge of the emulsion phase is measured.

Each induction probe is connected to a separate Kistler charge amplifier (model 5011B or 5015) by a coaxial cable. Although the induction probe is simple in concept, in practice it is susceptible to drift, charging, and distortion. Charge amplifiers and Teflon® insulation minimized the first two of these problems. Through the use of conductive shields, field distortion was minimized. Grounding of these shields, in combination with the very low potential of the probe, enabled optimal measurement of the fields generated by the charged particles. The outputs of the Kistler charge amplifiers were synchronously recorded using an LMS-Difa APB220 data-acquisition system at a sample rate of 200 Hz.

The four probes described above can measure induced charges during the passage of bubbles. Figure 3 shows typical experimental results for a bubble with its center passing probe 1 and the outer edge of the bubble passing probe 4. The measurement shows the change in induced charges, which has the opposite sign to the change in charges in front of the probe. When the bubble is far from the probes, the signals are constant. When the bubble nose approaches the probe, the induced charges began to decrease until a minimum was reached when the center of the bubble reaches the probe. Induced charges then increased as the bubble moved away from the probe. Maximum charges occurred after the bubble passed the three central probes 1, 2, and 3, but not probe 4. All induced charges reached stable values after the bubble left the probes far behind. Note that the "zero level " of charge is arbitrary—an absolute value cannot be determined using this technique. The purpose of this article is to reconstruct the charge distribution surrounding the bubble from the induced charge signals recorded from all four probes.

Reconstruction of Charge Distribution

The region around the bubble is first divided into a number of pixels, as shown in Figure 4. Combining Gauss's law with the definition of electric field and potential,[11] the electrostatic field E and potential V are given by

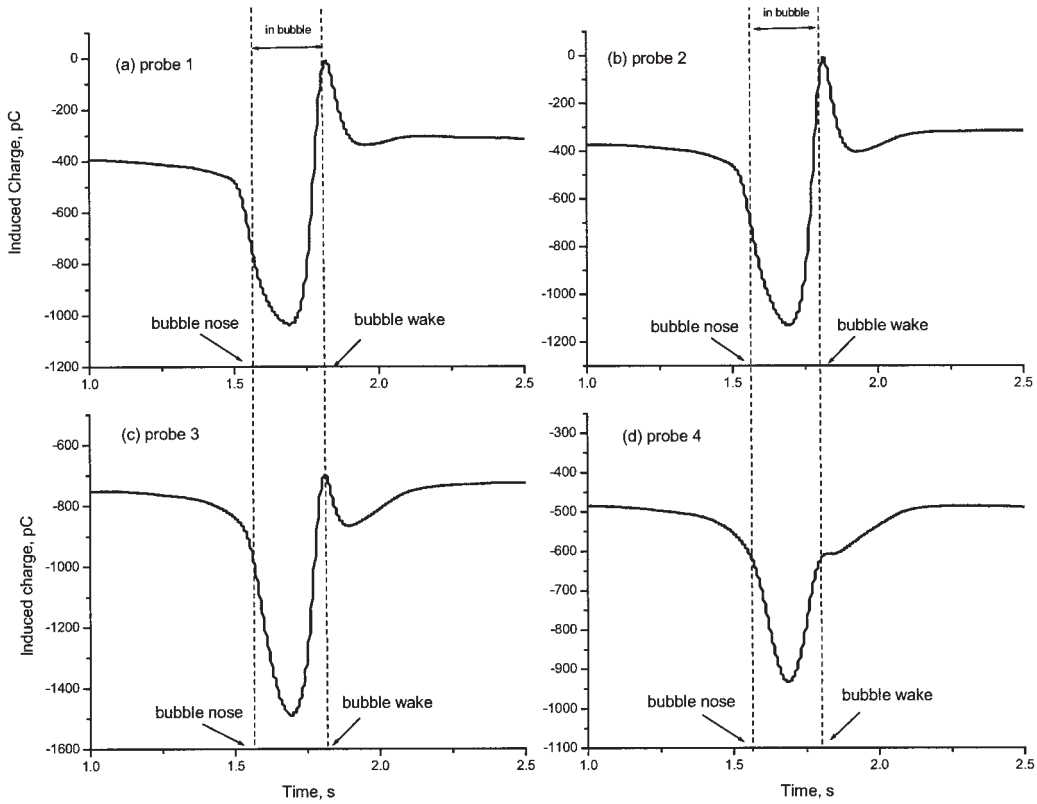

Figure 3. Induced charges measured by the four probes as a single bubble passed.

Approximate time of the passage of the bubble nose and wake are shown. The signal from probe 4 is weaker than the others because it was at the edge of the bubble.

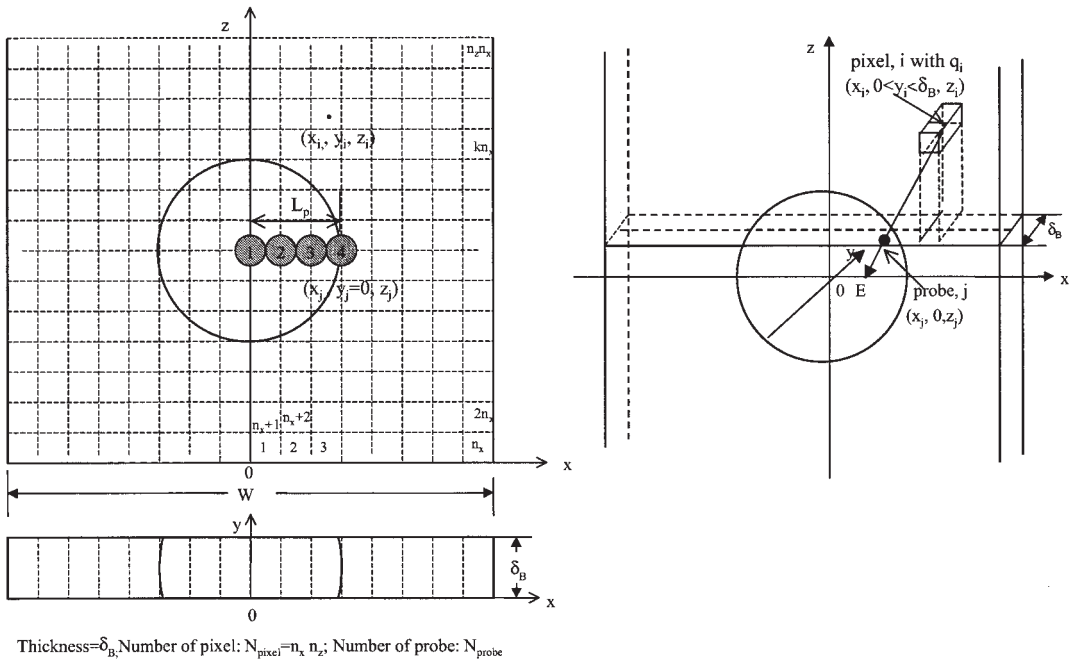

Figure 4. Geometric positions of the probes and pixel grid reconstruction.

$$\text{div } E = \frac{q}{\Pi} \tag{1}$$

and

$$E = -\text{grad } V \tag{2}$$

where q is the volume charge density and Π is the permittivity of the medium, assumed to be uniform in the region of interest.

From Eqs. 1 and 2

$$\text{div}(\text{grad } V) = \nabla^2 V = \frac{\partial^2 V}{\partial x^2} + \frac{\partial^2 V}{\partial y^2} + \frac{\partial^2 V}{\partial z^2} = -\frac{q}{\Pi} \tag{3}$$

It is assumed that there are charges only in pixel i with constant charge density q_i, in the y direction, and with no charges in other regions. Thus

- $q = q_i$ at $x = x_i$, $0 < y < \delta_B$, and $z = z_i$
- $q = 0$ in all other regions

Because the permittivity Π of the medium in the bed is taken to be uniform in all directions, and letting $v' = -(\Pi V/L_p^2 q_i)$, $x' = x/L_p$, $y' = y/L_p$, and $z' = z/L_p$, then the dimensionless form is

$$\frac{\partial^2 v'}{\partial x'^2} + \frac{\partial^2 v'}{\partial y'^2} + \frac{\partial^2 v'}{\partial z'^2} = q' \tag{4}$$

where

- $q' = 1$ at $x' = x_i/L_p$, $0 < y' < \delta_B/L_p$, and $z' = z_i/L_p$
- $q' = 0$ in all other regions

The boundary conditions are

- on the "left " and "right " sides: $x' = -W/2L_p$ and $x' = W/2L_p : v' = 0$
- at the front and rear walls: $y' = 0$ and $y' = \delta_B/L_p : v' = 0$
- at $z = 0$ and $z = H_{bed}/L_p : \partial v'/\partial z' = 0$

Equation 4 can be solved to obtain v' and thus V.

For an infinitesimal element of the probe at $(x_j, y_j = 0, z_j)$, the electric field perpendicular to the wall can be estimated by

$$E_\perp = E_y = -\left.\frac{\partial V}{\partial y}\right|_{x=x_j, y=0, z=z_j} \tag{5}$$

Then the induced charge on an infinitesimal element ds of the probe is

$$\sigma_{ij} = \Pi E_\perp ds = -\Pi \left.\frac{\partial V}{\partial y}\right|_{x=x_j, y=0, z=z_j} ds = q_i L_p \left.\frac{\partial v'}{\partial y'}\right|_{x'=x_j/L_p, y=0, z=z_j/L_p} ds \tag{6}$$

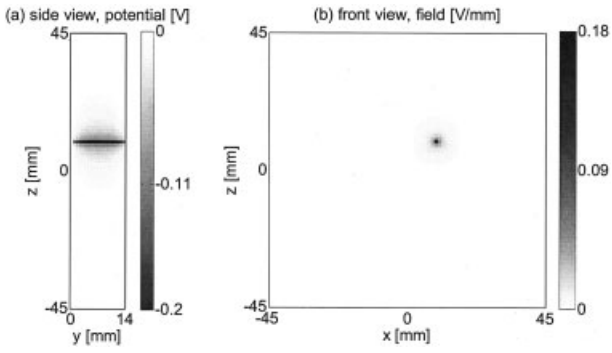

Figure 5. Electric potential over the cross section of the column (a) and the electric field perpendicular to the wall (b) resulting from a simulated line charge $-q/\Pi = 1$ C/(F mm^2) located at $x = 10$ mm and $z = 10$ mm.

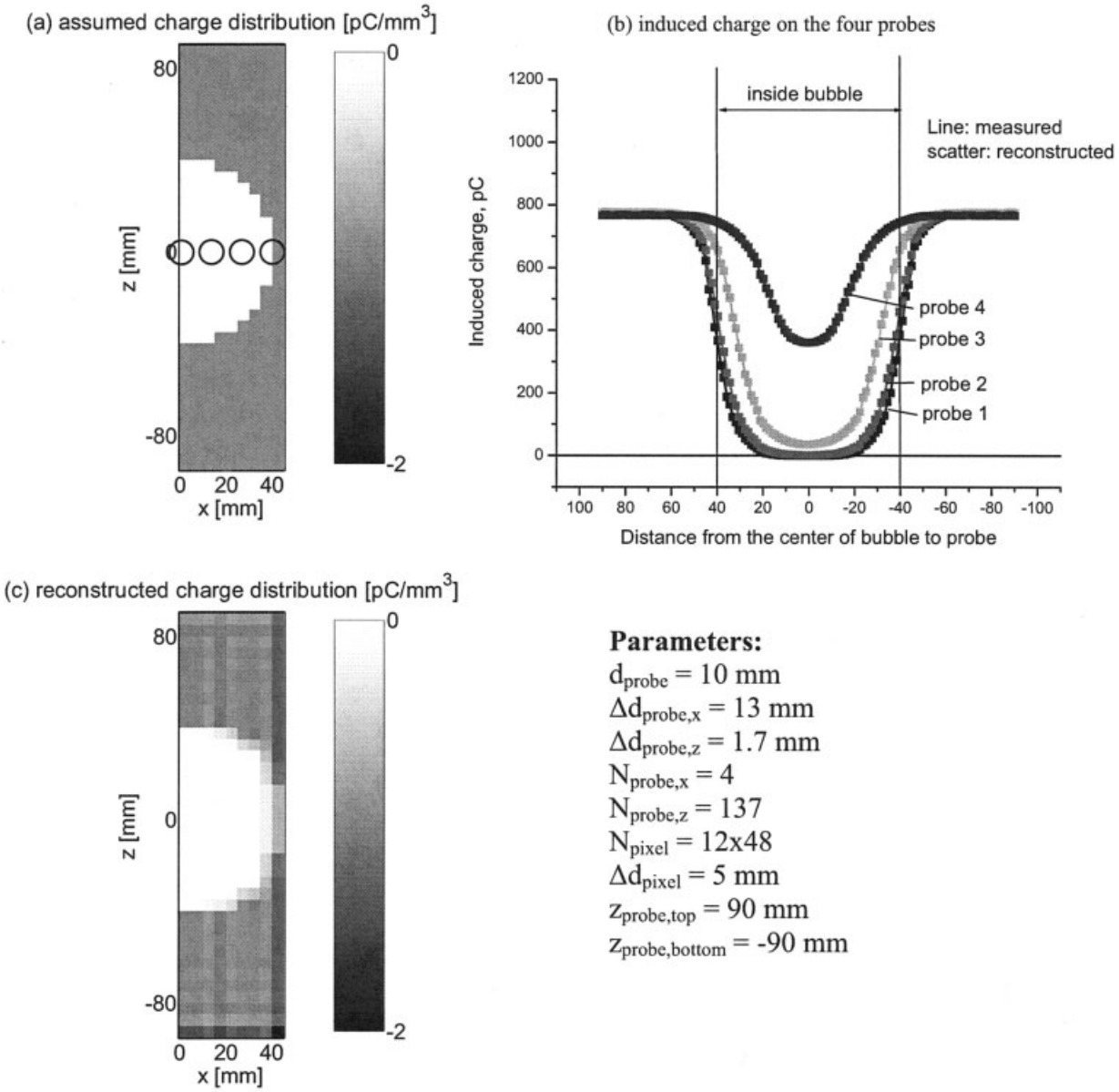

Figure 6. Simulation of a rising bubble (d_B = 80 mm) with a uniform charge of 1 pC/mm^3 assumed in the emulsion phase.

The simulated induced charges (b) are used to reconstruct the charge distribution (c). The positions of the induction probes are shown in (a).

The total charge on probe j is

$$\sigma_{ij,total} = \iint_{\text{surface of probe } j} \sigma_{ij} ds \tag{7}$$

If the probe is a circular plate of radius r_{probe} with its center at $(x_{j0}, 0, z_{j0})$, the total charge of probe j from the ith pixel can be expressed as

$$\sigma_{ij,total} = \iint_{\text{surface of probe } j} \sigma_{ij} ds = q_i L_p \int_{x_{j0}-r_{probe}}^{x_{j0}+r_{probe}} \int_{z_{j0}-[r_{probe}^2-(x_j-x_{j0})^2]^{0.5}}^{z_{j0}+[r_{probe}^2-(x_j-x_{j0})^2]^{0.5}} \left.\frac{\partial \nu'}{\partial y'}\right|_{x'=x_j/L_p, y'=0, z'=z_j/L_p} dz_j dx_j \tag{8}$$

Let

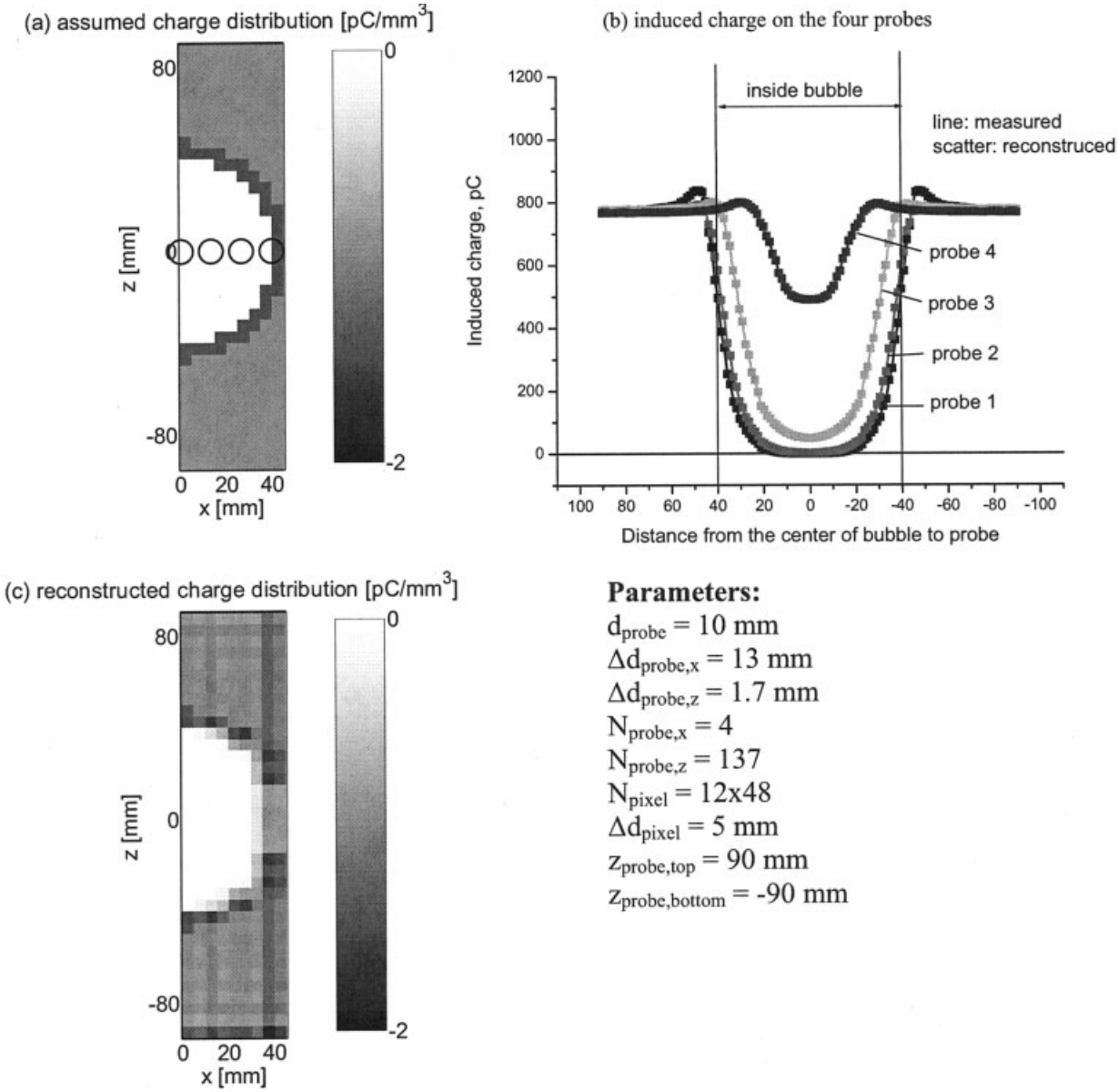

Figure 7. Second simulation of a rising bubble (d_B = 80 mm) with a uniform charge of 1 pC/mm^3 assumed in the emulsion phase, but now with a thin layer of highly charged particles (2 pC/mm^3) around the bubble.

The simulated induced charges (b) are used to reconstruct the charge distribution (c). The positions of the induction probes are shown in (a).

$$\omega_{ij} = L_p \int_{x_{j0}-r_{probe}}^{x_{j0}+r_{probe}} \int_{z_{j0}-[r_{probe}^2-(x_j-x_{j0})^2]^{0.5}}^{z_{j0}+[r_{probe}^2-(x_j-x_{j0})^2]^{0.5}} \left.\frac{\partial \nu'}{\partial y'}\right|_{x'=x_j/L_p,y'=0,z'=z_j/L_p} dz_j dx_j \tag{9}$$

Equation 8 is used to calculate the induced charge on probe j attributed only to pixel i having a charge density q_i. The induced charge from all pixels to probe j is then obtained by

$$Q_j = \sum_{i=1}^{N} \sigma_{ij,total} = \sum_{i=1}^{N} \omega_{ij} q_i \qquad (j = 1, 2, \ldots, M) \tag{10}$$

Theoretically, if the charge induced on probe Q_j can be measured, q_i for each pixel can be reconstructed using multiple probes. The quality of the reconstruction is influenced by the number of measurements and the number of probes. For good reconstruction, measurements should be taken inside, on the border, and outside the bubble. The larger the number of probes, the better the reconstruction.

In our experiments, only four probes were fixed horizontally on the wall and many (10,000) pixels had to be employed in the reconstruction (see Figure 4) to gain sufficient resolution. Ideally, one should install many probes surrounding the rising bubble to reconstruct the charge density distribution. For the current case with only four fixed probes, it is assumed that each

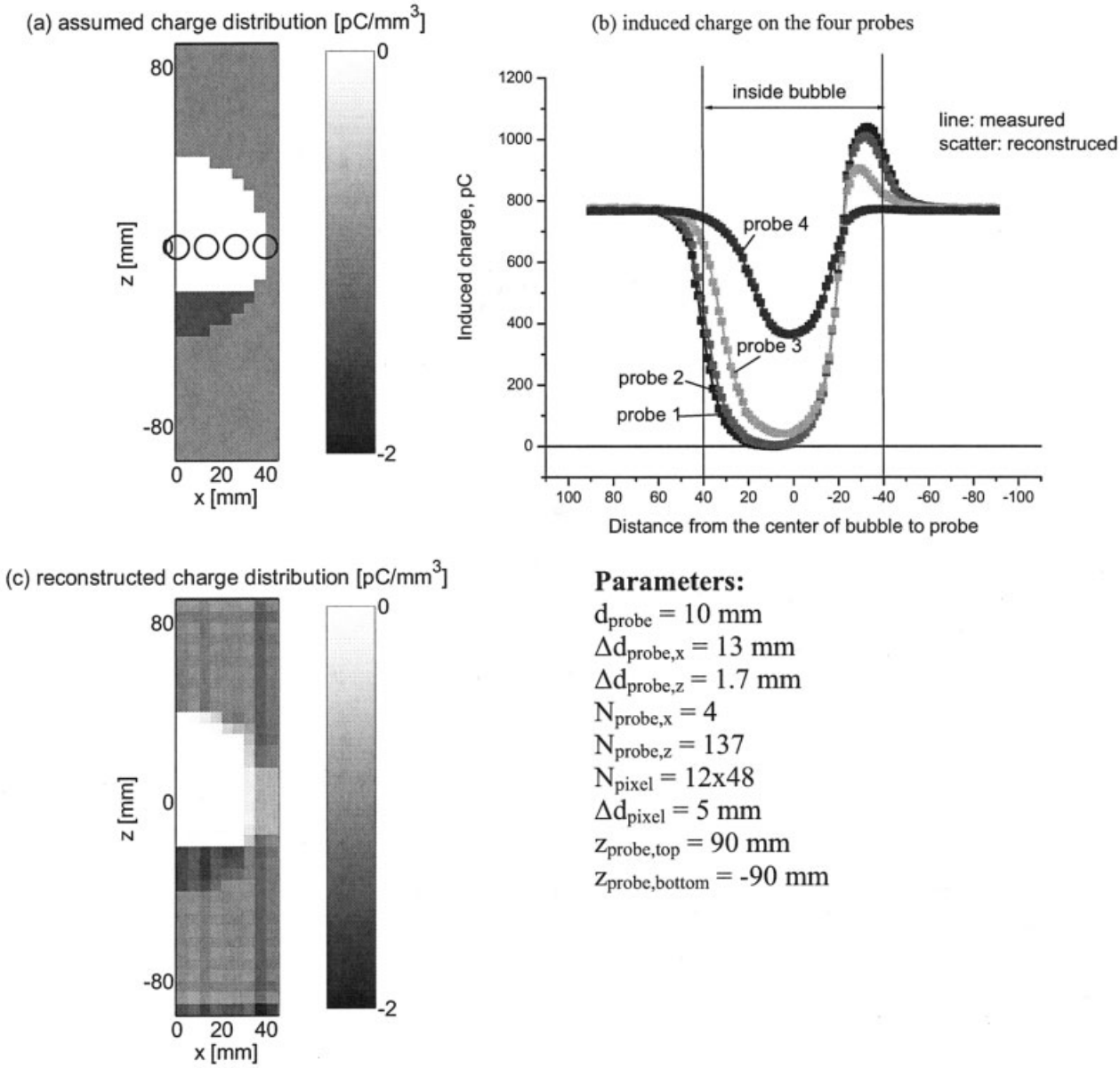

Figure 8. Third simulation of a rising bubble (d_B = 80 mm), with a uniform charge of 1 pC/mm^3 assumed in the emulsion phase and a highly charged wake (2 pC/mm^3).

The simulated induced charges (b) are used to reconstruct the charge distribution (c). The positions of the induction probes are shown in (a).

bubble is symmetrical and that the charge around the bubble does not vary as the bubble passes through the measurement region. The latter assumption means that the rising of the bubble past the probes provides the vertical resolution, and the number of probes limits only the horizontal resolution. Thus, although there were only four probes, the induced charge measured at different vertical locations relative to the bubble can be obtained and used to solve Eq. 10.

Simulation Results

The model was implemented in Fortran using Visual FORTRAN Professional Edition 5.0. Simulations were performed using a line charge and various charge distributions around bubbles to test the model and ascertain how effective it is in reconstructing the charge distribution.

First, the electric field around a line of charge leading from the front wall to the back wall of the column of $-q/\Pi = 1$ C/Fmm^2, situated at $x = 10$ mm and $z = 10$ mm, was determined. The rest of the domain is uncharged. The result is presented in Figure 5. Figure 5a shows the electric potential from the side—it is clear that the potential distribution is very narrow at $z = 10$ mm. Figure 5b shows the electric field from the front. Based on this simulation it is concluded that the charge induced on a properly shielded probe situated flush with the wall arises primarily from charges in the region directly in front of it. This implies that matrix ω_{ij}, required to reconstruct

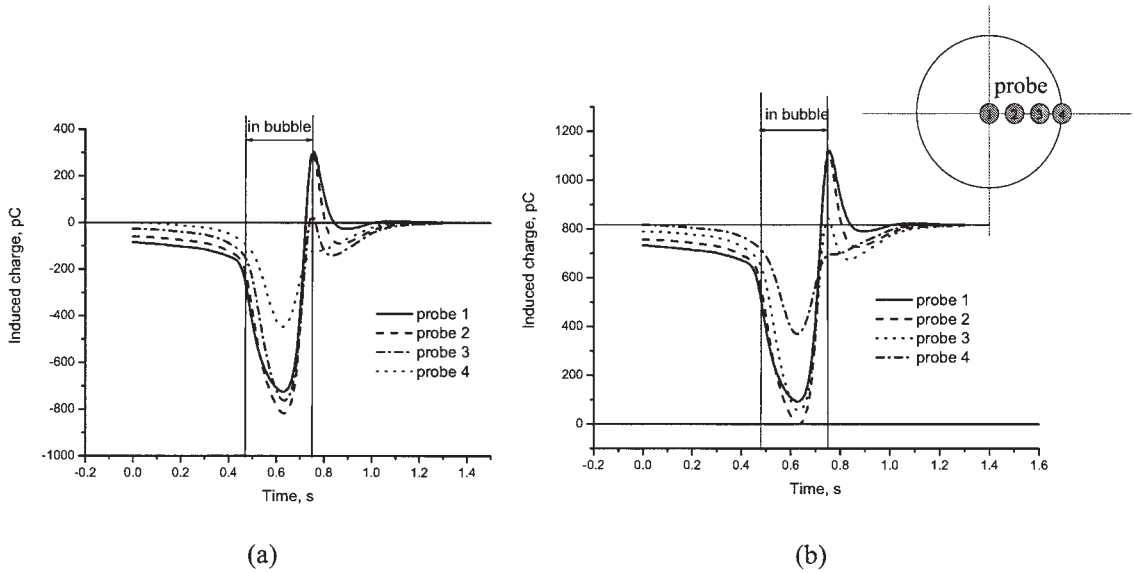

Figure 9. Scaling of the measured induced charges to a common baseline.

(a) Charges for all four probes after the bubble has advanced far beyond the probes are set to zero. (b) The minimum induced charge for probe 2 while the probe is at the center of the bubble is set to zero.

the charge distribution q_i in Eq. 10, is singular as a result of the sharp gradient in the electric field. To solve Eq. 10, matrix ω_{ij} was calculated and then inverted. The LSGRR subroutine was used to invert the matrix directly, but if the matrix was determined to be mathematically singular or ill-conditioned, a least-squares routine or the singular value decomposition routine provided by Visual FORTRAN Professional Version 5.0 was used to obtain approximate results.

Next, a bubble with its associated charge distribution passing the probes was simulated, and the induced charge was used to reconstruct the original charge distribution. The diameter of the bubble was set at 80 mm for four probes of diameter 10 mm located horizontally, as shown in Figure 1. The distance between adjacent probes is 13 mm, in the experiments. It was assumed there is a uniform charge distribution in the emulsion phase (around the bubble) of $q = 1$ pC/mm^3 and that the inside of the bubble was uncharged. The simulated and reconstructed charges are presented in Figure 6. The charges induced on the four probes, shown in Figure 6b, are seen to be symmetric and to have the same value when the bubble is far away. When the simulated bubble approaches the probes, the induced charges begin to decrease, reaching a minimum when the bubble is directly in front of the probes. As the edge of the bubble approaches the probes, the induced charges again increase. The induced charges for probes 1 and 2 are 0 and for probe 3 are close to 0 when probes are at the center of the bubble because of zero charge inside the bubble. The induced charge for probe 4, which is at the edge of the bubble, is not zero. Using these four calculated induced charges, the charge distribution around the bubble is reconstructed with the above model and shown in Figure 6c. It can be seen that there is reasonable agreement between the assumed and reconstructed charge distributions. The distortion at the edge, around probe 4, is largely a result of the ill-defined matrix ω_{ij} while solving Eq. 10.

In the second simulation, we test whether the reconstruction can accurately reproduce a thin highly charged layer of parti-

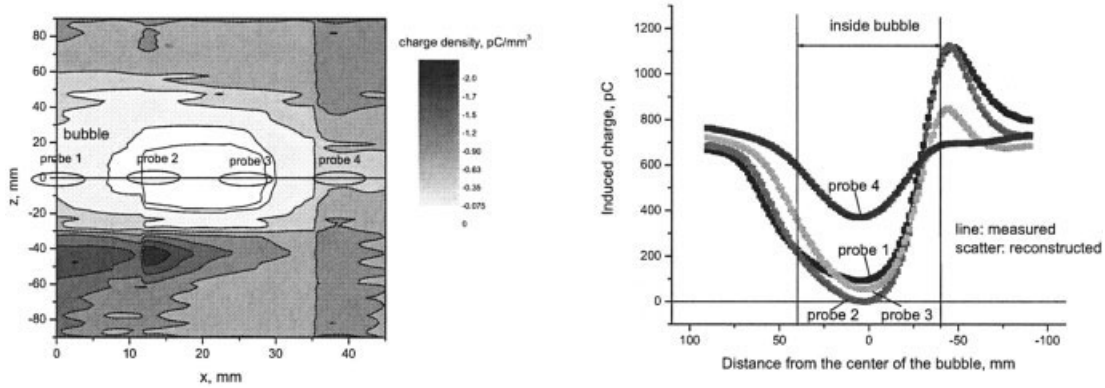

Figure 10. (a) Reconstructed charge distribution and (b) comparison of measured induced charge signals and simulated induced charge signals based on reconstructed charge distribution.

Case 1: $H_{mf} = 0.7$ m, $d_B = 0.08$ m, $u_B = 0.45$ m/s, $d_p = 565$ μm, $\rho_p = 2500$ kg/m^3, $Q_{air} = 1.78$ m^3/s.

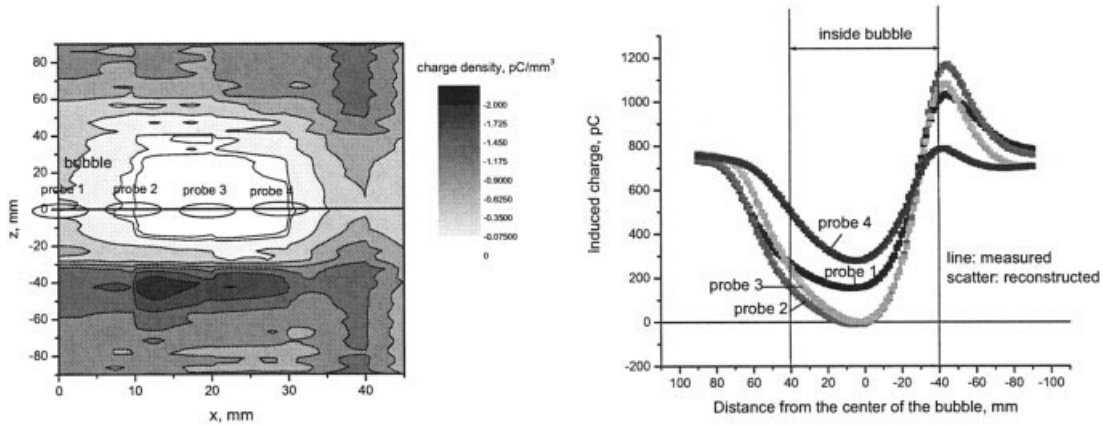

Figure 11. (a) Reconstructed charge distribution and (b) comparison of measured induced charge signals and simulated induced charge signals based on reconstructed charge distribution.

Case 2: $H_{mf} = 0.7$ m, $d_B = 0.08$ m, $u_B = 0.45$ m/s, $d_p = 565$ μm, $\rho_p = 2500$ kg/m^3, $Q_{air} = 1.78$ m^3/s.

cles around the bubble. In a two-dimensional view, this means that a ring of particles surrounds the bubble with a higher charge than that of the emulsion phase. Figure 7 shows the induced charges for the four probes (7b) and the reconstructed charge profile (7c) with the distribution assumed to have a thin, highly charged layer around the bubble (7a). It can be seen in Figure 7b that there are peaks when the simulated bubble reaches and leaves the probes and that the induced charges for probes 1, 2, and 3 are close to zero when the center of the bubble passes the probes. The induced charge for probe 4 when the bubble center passes is larger than the others because the probe is right at the edge of the bubble. It can also be seen from Figure 7c that there are differences between the reconstructed charge and the assumed charge distribution, especially in the highly charged layer around the bubble. Because there is no probe in the region outside the bubble, the charge reconstruction is poor for $x > 40$ mm. Adding one or two probes outside the bubble would substantially improve the reconstruction.

When a higher charge density is assumed in the wake region of the bubble, as shown in Figure 8a, it can be seen from Figure 8b that the calculated induced charges for probes 1, 2, and 3 reach maxima as the wake of the bubble passes the probe. All the induced charges approach the same base value after the bubble moves away. These induced charge profiles are very similar to the preliminary experimental results shown in Figure 3. Again, the induced charges for probes 1, 2, and 3 are zero when the center of the bubble passes the probes, whereas the induced charge for probe 4 has values greater than zero. The higher charge density in the bubble wake region is captured in the reconstructed profile in Figure 8c, although discrepancies still exist between the assumed and reconstructed charge distributions.

Reconstruction of Experimental Signals

Typical induced charge measurements using the experimental setup are presented in Figure 3. We now reconstruct the charge distribution in the same way as in the simulated cases presented above, but with experimentally measured charge signals as the input.

The baseline of the measured induced charge (that is, charge of the emulsion phase) cannot be measured using the induction probes, but must be determined to reconstruct the charge distribution around bubbles. This is based on observations in the previous section that (1) induced charges from the four probes have the same base value when the bubble is far from the probes; (2) the minimum charge induced on the probes as the bubble passed (probes 1, 2, and 3) may reach zero; and (3) the induced charge for a probe on the edge of, or outside, the bubble (probe 4) should be nonzero. Lines for all four probes after the bubble advanced far beyond the probes are first set to zero as shown in Figure 9a. The minimum induced charge for probe 2 while the center of the bubble passes the probe is found to have the lowest value. Thus, the scale is adjusted so that the minimum induced charge of probe 2 is set to zero. The final rearranged induced charge signals are shown in Figure 9b. All induced charges from the four probes have the same base value of approximately +820 pC when the bubble is far from the probes.

In the reconstruction model presented above, it is assumed that a bubble is symmetric and that the charge around the bubble does not change as the bubble rises. Therefore, the induced charge as a function of time can be converted into a series of induced charges varying with vertical distance between the center of the bubble and the probe. Here, data from 0.45 to 0.85 s, or the vertical distance between the center of bubble and the probe from 90 to -90 mm, are chosen for the reconstruction.

Figure 10a shows the reconstruction results for the induced charges shown in Figure 9. It can be seen that the charge inside the air bubble is almost zero, whereas the charges in the dense phase remote from the bubble is negative. There is a more negatively charged wake, confirming the postulate based on measurements with a single collision probe.[7,9] However, there is no layer of higher charge density in the boundary region around the bubble-dense phase interface, contrary to the assumption of a surface charge distribution made in the models used to interpret the collision probe data.[7,9] The charge density outside the bubble in the dense phase is approximately -0.9 pC/mm^3 or -3.6×10^{-7} C/kg. The charge in the wake is about -1.7 pC/mm^3 or -6.8×10^{-7} C/kg. Figure 10b compares measured induced charges with those calculated from the re-

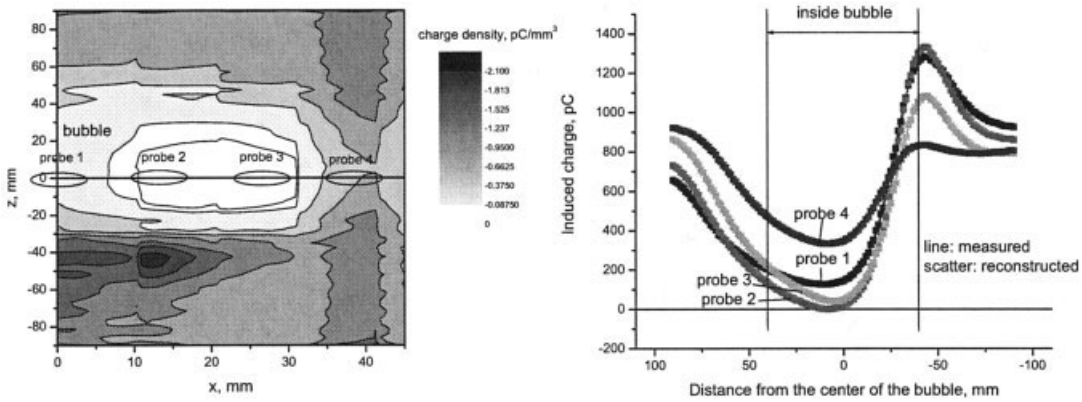

Figure 12. (a) Reconstructed charge distribution and (b) comparison of measured induced charge signals and simulated induced charge signals based on reconstructed charge distribution.

Case 3: H_{mf} = 0.7 m, d_B = 0.08 m, u_B = 0.45 m/s, d_p = 565 μm, ρ_p = 2500 kg/m^3, Q_{air} = 1.78 m^3/s.

constructed charge density in Figure 10a. As expected, the differences are not significant.

The reconstruction of other typical bubbles (see Figures 11 and 12) gives similar charge density distribution profiles, confirming that the emulsion phase with glass beads is negatively charged with a more negatively charged wake.

Conclusions

A technique has been developed to determine the charge distribution around a single rising bubble in a two-dimensional fluidized bed using a number of induction probes positioned flush with the outer wall of the Plexiglas® column. With the probes at the same level, the vertical resolution is obtained by the rise of the bubble under the assumption that the charge distribution does not change during the bubble passage. The method currently uses four probes of 10-mm diameter, but the resolution of the charge density distribution reconstruction can be improved by reducing the probe size and increasing the number of probes. The reconstruction technique does not require any a priori model or knowledge about the charge distribution or density.

Reconstructed images from experimental data show that the emulsion phase far from the bubble was charged negatively for the glass beads used in the experiments. There is a decrease of charge density moving inward from the emulsion phase bubble interface, with essentially zero charge density inside the air bubble. However, the charge distribution has been shown to be nontrivial for this system in that the particles in the wake are strongly charged. It remains for future work to demonstrate the effect of this on the general charging of the bed mass, as well as to show the influence of material properties.

Acknowledgments

The authors are grateful for support from the Natural Sciences and Engineering Research Council of Canada (NSERC) and Nova Chemicals of Canada. F. Kleijn van Willigen is also grateful for the support from Profs. J. van Turnhout and C. M. van den Bleek (Delft University of Technology) for his work at the University of British Columbia.

Notation

d = diameter, m
Δd = differential distance, m
E = electric field, V/m
$E_\perp$ = electric field perpendicular to wall, V/m
H_{bed} = fluidized bed height, m
H_{mf} = packed bed height, m
L_p = distance between probes 1 and 4 (see Figure 4), m
M = number of pixels
N = number of probes
q = volumetric charge density, C/m^3
Q = induced charge on probe from all pixels, C
Q_{air} = air flow rate, m^3/s
r = radius, m
s = area, m^2
u = velocity, m/s
$v' = -(\Pi V/L_p^2 q_i)$
V = electric potential, V
W = width of two-dimensional bed, m
x, y, z = Cartesian coordinates, z = vertical, y = horizontal, x = width, m
x', y', z' = normalized coordinates, $x' = x/L_p$, $y' = y/L_p$, $z' = z/L_p$

Greek letters

δ_B = thickness of two-dimensional column, m
σ = induced charge on probe from one pixel, C
Π = permittivity of medium, F/m
ρ = density, kg/m^3
ω = matrix in Eq. 10

Subscripts

B = bubble
i = ith pixel
j = jth probe
x, y, z = x, y, and z directions
p = particle

Literature Cited

1. Harper WR. *Contact and Frictional Electrification*. Oxford, UK: Oxford Univ. Press; 1967.
2. Zhao H, Castle GSP II, Inculet Bailey AG. Bipolar charging of poly-disperse polymer powders in fluidized beds. *IEEE Trans Ind Appl.* 2003;39:612-618.
3. Mehrani P, Bi HT, Grace JR. Electrostatic charge generation in gas–solid fluidized beds. *J Electrostat.* 2005;63:165-173.

4. Chen AH, Bi HT, Grace JR. Measurement of particle charge-to-mass ratios in a gas–solids fluidized bed by a collision probe. *Powder Technol.* 2003;135/136:181-191.
5. Murtomaa ME, Räsänen E, Rantanen J, Bailey A, Laine E, Mannermaa J-P, Yliruusi J. Electrostatic measurements on a miniaturized fluidized bed. *J Electrostat.* 2003;57:91-106.
6. Boland D, Geldart D. Electrostatic charging in gas fluidized beds. *Powder Technol.* 1971/1972;5:289-297.
7. Park A-H, Bi HT, Grace JR, Chen A. Modeling charge transfer and induction in gas–solid fluidized beds. *J Electrostat.* 2002;55:135-168.
8. Park A-H, Bi HT, Grace JR. Reduction of electrostatic charges in gas–solid fluidized beds. *Chem Eng Sci.* 2002;57:153-162.
9. Chen AH, Bi HT, Grace JR. Effects of charge distribution around bubbles on charge induction and transfer to a ball probe in gas–solid fluidized beds. *J Electrostat.* 2003;58:91-115.
10. Taylor DM. Measuring techniques for electrostatics. *J Electrostat.* 2001;51:502-508.
11. Cross J. *Electrostatics: Principles, Problems and Applications*. Bristol, UK: Hilger; 1987.

Manuscript received May 4, 2004, and revision received May 25, 2005.